JOURNAL OF MATERIALS SCIENCE **33** (1998) 5517–5533

Hot isostatic pressing of metal reinforced metal matrix composites

A. L. FILHO, H. ATKINSON, H. JONES
Department of Engineering Materials, Hadfield Building, University of Sheffield, Mappin St., Sheffield, S1 3JD, UK
E-mail: h.v.atkinson@shef.ac.uk

E. DE LOS RIOS
Department of Mechanical Engineering, University of Sheffield, Mappin St., Sheffield, S1 3JD, UK

S. KING
Bodycote HIP Ltd., Carlisle Cl., Sheffield Rd., Sheepbridge, Chesterfield, S41 9ED, UK

Metal reinforced Metal Matrix Composites (MMMCs) made by combining an aluminium alloy matrix with stainless steel reinforcing wires are potentially cheaper and tougher than continuous fibre ceramic reinforced Metal Matrix Composites (MMCs). Although they do not give as great enhancements in stiffness and strength, worthwhile gains are achieved. Such MMMCs can be produced by Hot Isostatic Pressing (HIPping), which reduces interfacial reactions in comparison with liquid metal routes. Here, stainless steel (316L) and commercial purity aluminium wires were used to make bundles which were inserted into mild steel cans for HIPping at 525 °C/120 min/100 MPa. Some stainless steel wires were pre-coated with A17Si, to examine the effect of coatings on mechanical properties. Specimens were evaluated in terms of their tensile and fatigue properties. During HIPping, cans collapsed anisotropically to give different cross-section shapes, and for larger diameter cans, there was also some longitudinal twisting. Wires tended to be better aligned after HIPping in the smaller diameter cans, which produced material having higher modulus and UTS. Higher volume fractions of reinforcement tend to give better fatigue properties. Composites with coated stainless steel wires gave higher composite elongation to failure than uncoated wires. Both uncoated and coated wires failed by fatigue during fatigue testing of the composite. This contrasts with ceramic reinforced MMCs where the fibres fracture at weak points and then pull out of the matrix.

1. Introduction

Metal reinforced Metal Matrix Composites (MMMCs) are gaining increasing attention for applications in industry [1]. Aluminium alloys reinforced with continuous stainless steel wires would combine the light weight of aluminium with the strength, stiffness and higher temperature capabilities of stainless steel. The enhancements in specific properties are not as large as for continuous fibre ceramic reinforced alloys (Table I). Nevertheless, in relation to the unreinforced matrix, there are worthwhile gains, particularly in specific strength. In addition, the toughness and the elevated temperature properties are expected to be better than the ceramic reinforced materials.

In the 1960s and 1970s, considerable work was carried out on aluminium alloy/stainless steel combinations processed both by solid state [2–7] and by liquid metal routes [8–10]. For the liquid metal routes, the reactions at the interfaces between the molten aluminium and the stainless steel were generally extensive and detrimental. Bhagat and co-workers studied the formation and growth kinetics of interfacial intermetallic compounds for both liquid metal and solid state routes [11, 12]. In the 1990s, interest was renewed. For example, Colin *et al*. [13] and Delannay *et al*. [14] made squeeze-cast A1-MMMCs reinforced with twelve micron stainless steel fibres. They controlled the extent of interfacial reaction via the infiltration parameters and the volume fraction of fibres. Barbier and Ambroise [1] found that a squeeze cast stainless steel short fibre A1 MMC had a tensile strength 3 to 4 times that of the A1 matrix manufactured under the same conditions. The commercial interest is typified by Honda, who produced a squeeze-cast stainless steel wire reinforced aluminium con-rod for one of its home market, small family cars [15]. A 30% weight saving was achieved with improvements in engine power and fuel economy [16]. Recent studies have focussed on producing aluminium/stainless steel composites by hot pressing [17, 18] and extending the work towards reactive

TABLE I Specific properties of commerical purity aluminium and 316L stainless steel compared with those for Al 30 vol % 316L and Al 30% SiC calculated by the rule of mixtures

	Young's modulus, E (GPa)	Yield strength, σ (MPa)	Density ρ (kg m^{-3})	Melting point (K)	Specific modulus, E/ρ (GPa kg^{-1} m^3)	Specific strength, σ/ρ (MPa kg^{-1} m^3)
Al (1100)	70	170	2700	933	0.03	0.06
Stainless steel 316L	200	$\sim$800	8000	—	0.03	0.1
SiC (Nicalon)	45–480[a]	300–4900[b]	2800	1573	0.125	1.1
Al 30 vol % 316L	109	359	4290	—	0.03	0.08
Al 30 vol % SiC	154	1019	2730	—	0.06	0.4

[a]Take 350 GPa as a representative value.
[b]Take 3000 MPa as a representative value.

processing of stainless steel coated with nickel and hot pressed with aluminium to give a stainless steel/NiA1 composite [19].

In general, liquid metal based routes give some interfacial reaction products, which tend to degrade the mechanical properties. Solid state routes such as hot die pressing and Hot Isostatic Pressing (HIPping) should inhibit such reactions. In addition, one of the advantages of a route involving matrix plastic flow during consolidation is that the oxide layer on the aluminium will tend to be broken up, allowing diffusion bonding to take place [20]. Results on HIPping of continuous fibre Metal-reinforced MMCs have not previously been reported.

HIPping involves the simultaneous application of a high pressure (usually inert) gas and an elevated temperature in a specially constructed vessel [21]. The pressure applied is isostatic because it is developed in a gas, so that, at least as a first approximation, no alteration in component geometry should occur. The results in this work however show severe anisotropic deformation and the reasons for this will be discussed. Under the heat and pressure, internal pores or defects within the solid body collapse and weld up.

In this work, bundles of aluminium and stainless steel wires were prepared and vacuum canned prior to HIPping. Some of the stainless steel wires were precoated with A17.3Si to examine the effect on mechanical behaviour after consolidation. After HIPping, specimens were tensile and fatigue tested. The shape of the can, distribution of reinforcement and interfacial reactions after HIPping were examined in order to interpret the mechanical properties.

2. Experimental

2.1. Pre-coating of stainless steel wires

Some wires were pre-coated with A17.3Si alloy (all compositions are given in wt %) in a laboratory rig. The wire was drawn through a bath of molten aluminium alloy (700 °C) continuously. A protective atmosphere of argon gas was running at approximately 6 l/min. The wire was pre-cleaned with one container of soap solution and one of alcohol. A ceramic die controlled the coating thickness at the exit from the bath. The coating was fully solidified before the wire was wound manually on to a spool.

2.2. Bundle preparation

Bundles were prepared from type 316L stainless steel (16.85 Cr, 10.33 Ni, 2.58 Mo, 0.42 Si, 0.42 Mn, 0.029 C, 0.016 P, 0.001 S bal. Fe) and aluminium alloy for HIPping by a method based on that described by Berghezan [22]. Lengths of 316L (coated for some bundles and uncoated for others) and aluminium alloy were cut from spools of wire and each one was straightened manually. Various bundles were then prepared (see Fig. 1). In the simplest arrangement (termed here Wire-Matrix i.e. W-M), two strips of sellotape were placed a set distance apart and the wires were laid down between the strips, alternating stainless steel and aluminium. The strip was then wound up to form a bundle. A more complex arrangement was to alternate one stainless steel wire with two aluminium wires (termed W-M-M-W). This was adopted as a first step to prevent stainless steel wires touching, an issue which emerged after the initial experiments with the W-M arrangement. A further development to prevent touching was to lay the wires on an aluminium foil backing so that each layer of wires was separated when the bundle was rolled up. This is termed the Foil-Wire-Matrix (F-W-M) arrangement. After the bundle had been produced it was wound tightly with aluminium wire around the outside and the ends attached to the sellotape cut off to avoid organic contamination during HIPping. Fig. 2 shows photographs of the (F-W-M) arrangement and of the bundle.

Bundles were made with commercial purity (0.6 mm in diameter) aluminium wires. The stainless steel wires were of different diameters for different bundles, some 0.3 mm diameter uncoated, some 0.5 mm coated and uncoated. The aluminium foil (A1 0.2Fe) was 0.15 mm thickness and had been prior annealed at 250 °C to facilitate rolling up the bundle. The aim of using different diameters was to examine the effect of varying volume fraction on the mechanical properties.

One bundle was prepared from commercial purity aluminium wires (0.6 mm in diameter) and foil without any reinforcing stainless steel wires, to act as a control.

Hand lay-up as described is labour intensive and clearly would not be economic for commercial

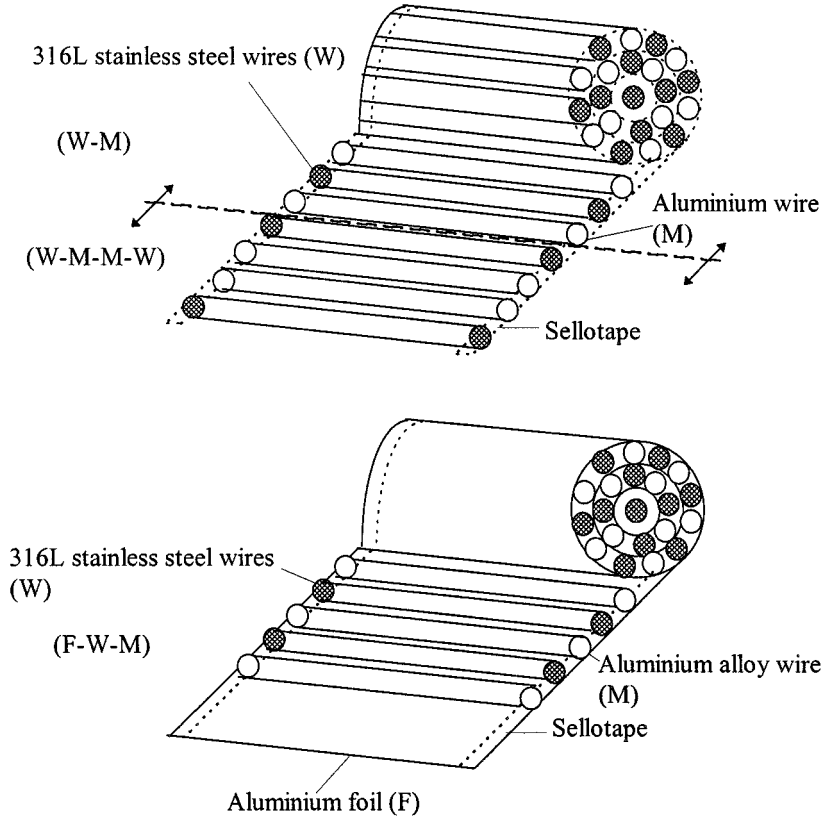

Figure 1 Schematic diagram of wire-matrix (W-M), wire-matrix-matrix-wire (W-M-M-W), and foil-wire-matrix (F-W-M) bundle arrangements.

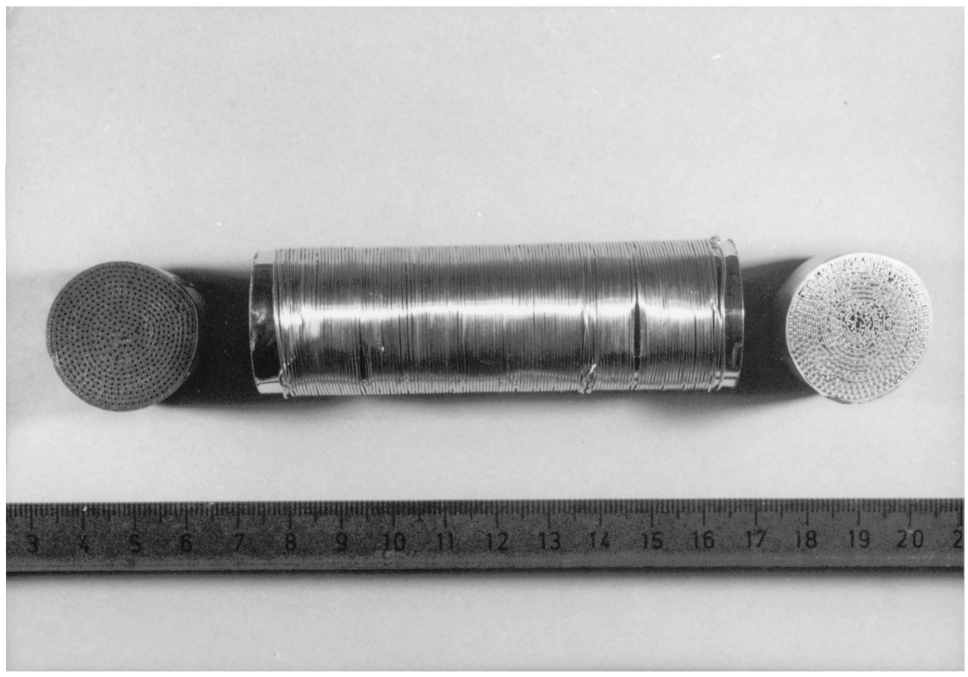

Figure 2 Bundle arrangement (F-W-M). 0.5 mm 316L stainless wires are dark spots in the cross-section and are separated by 0.6 mm aluminium wires (white spots) and 0.15 mm thick aluminium foil.

applications. However, it does allow different arrangements to be investigated from an experimental point of view.

2.3. Bundle consolidation by HIPping

Each bundle (9.5 cm in length) was placed in a steel can (specification C 0.20 wt%, Si 0.10–0.35 wt%, Mn 0.60–1.00 wt%, P & S 0.05 wt%) which was vacuum degassed, sealed by welding and HIPped at 525 °C/120 min/100 MPa. The heating rate was just under 10 °C/min and the full consolidation load was reached after about 70 minutes. The HIPping was carried out in an Autoclave Engineers laboratory unit at Bodycote HIP Ltd., Chesterfield, UK. The inner diameter of the cans (12, 18, 20, 26 and 28 mm) was as close as possible to the outer diameter of the bundle. However, inevitably there was some clearance between

the bundle and the can. The bundle would then be positioned off-centre at the beginning of HIPping, contributing to the uneven deformation reported later in Section 3.

2.4. Mechanical testing

Flat specimens for both tensile and S-N fatigue tests were cut by spark erosion machining from the HIPped bundles. The dimensions were non-standard because of the small overall dimensions of the HIPped composites. Fig. 3a shows samples cut by this method from one bundle with a ground surface finish obtained manually using 1200 grit paper and Fig. 3b the dimensions of the parallel-sided specimens for use with the extensometer. Tabs were prepared from cold-rolled aluminium sheets. These were designed to reduce peak specimen stress and to avoid grip penetration into the composite. Redux 403-Epoxy Paste Adhesive was employed, chosen because of its suitable properties for this work, as discussed by Greaves *et al*. [23]. For the work described here, a facility was developed for sticking tabs i.e. with a glass slide and double-sided sellotape adhered on its surface, which provided good alignment. The first samples were of reduced length gauge ($2 \times 4.6 \times 45$ mm) and, therefore, strain gauges (type EA-06-060LZ-120) were used to monitor the elongation. The majority of samples were longer ($2 \times 4.6 \times 60$ mm) and were tensile tested using an extensometer (type Instron 2620-604) on an Instron 8501 Machine with a 1000N to maximum load scale. The machine was set to stop the tensile test after an elongation of 10 mm was achieved at a constant speed of 0.2 mm/s. This is in agreement with the Standard Test Method for Tensile Properties of Fiber-Reinforced Metal Matrix Composites (ASTM D 3552-77). Axial loading fatigue testing was carried out on the same Instron machine at room temperature. Only 3 or 4 samples were available for fatigue testing from each HIPped bundle. Inevitably, therefore, the scatter in the results is large. A uniaxial load was applied with a stress ratio of 0.1 at a frequency of 10 Hz. A positive stress ratio was chosen due to the slenderness of the

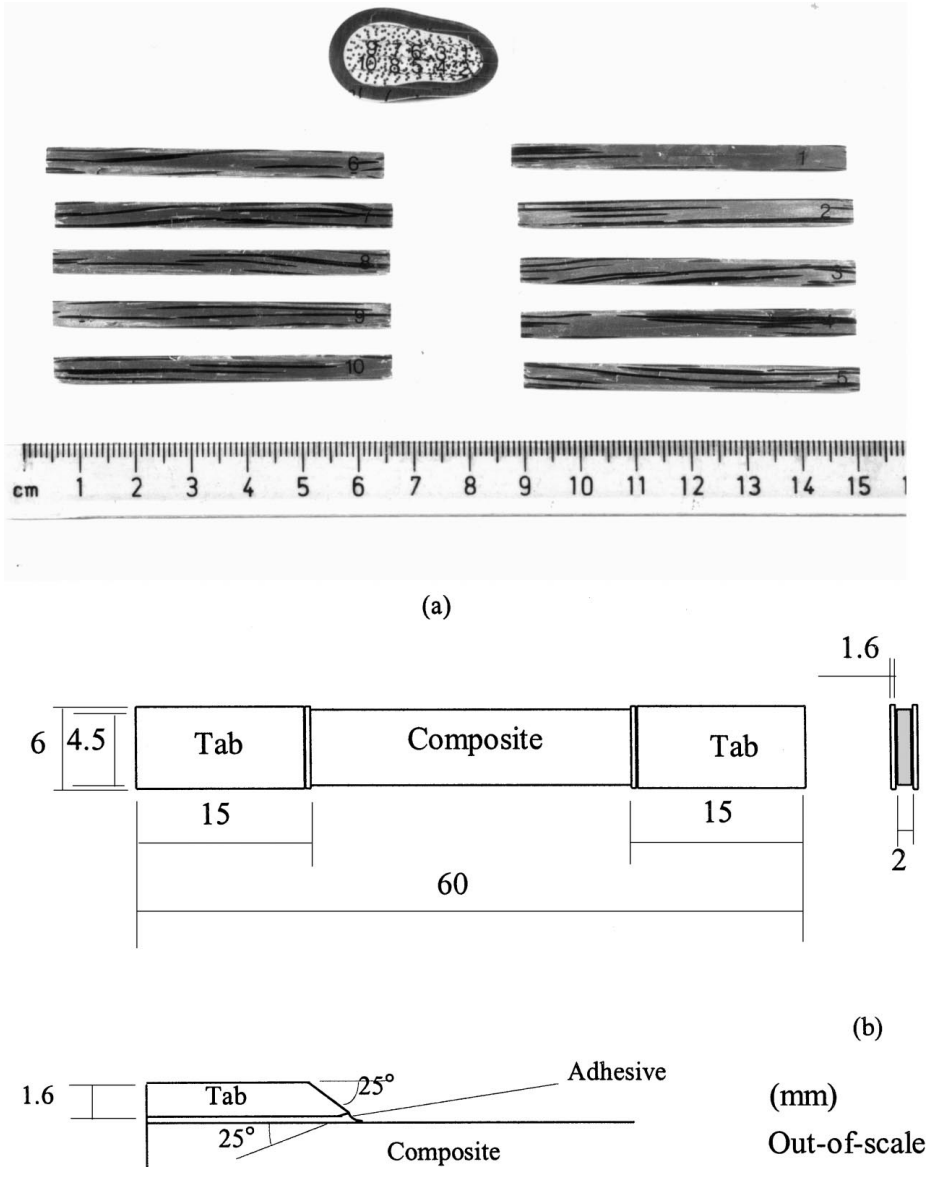

Figure 3 (a) Specimens cut by spark erosion machining from the (W-M-M-W) HIPped composite (0.5 mm uncoated 316L S.S. wire and 0.6 mm pure aluminium wire) in a 20 mm can. The speciments are ready for affixing the cold-rolled sheet aluminium tabs. The 316L wires are not well-aligned after HIPping: this will affect the mechanical test results. (b) General dimensions of parallel-sided speciment design for use with an extensometer.

specimens, which might have buckled if the stress ratio was negative. A scanning electron microscope (SEM CamScan Series 2) was utilised to examine the fracture mode in tensile and fatigue tests.

2.5. Optical metallography, microhardness testing and energy dispersive spectrometry

Composites can be difficult to prepare for metallography. Long periods of polishing and high pressure can cause relief between the matrix and the reinforcement. Here the procedure adopted was as follows: grinding on 240 grit paper to obtain a flat surface (300 rpm); grinding with 600 grit and 1200 grit for 1 min (300 rpm); polishing with 6, 3 and 1 μm diamond paste (oil-based) for 2 min (150 rpm); polishing with colloidal silco (water lubricant) for 2 min, and in water for 1 min on the same cloth to remove the silco particles adhered on the surface of the samples. Ultrasonic cleaning was used between each step. The samples were observed unetched in a Reichert-Jung-Polyvar-Met microscope to determine the quality of the interfaces and the reinforcement distribution. Image analysis was carried out in an AMS/Optomax V to find the reinforcement volume fraction and the number of W-W contacts relative to the total number of stainless steel wires in a given area (17.5 mm^2).

Microhardness testing was carried out on samples before and after HIPping using a Leco M-400 facility with a load of 100 gf applied for 10 s.

Interfacial reaction products were analysed by Energy Dispersive Spectrometry (EDS) on polished cross-sections in the SEM with a LINK AN 10000 system. Results were ZAF corrected and pure metal standards used for Fe, Cr, Ni, Mo, Mn, and Cu. Compound standards of $A1_2O_3$, $CaSiO_3$ and MgO were used respectively for A1, Si and Mg analysis.

3. Results

3.1. Interfacial reaction during pre-coating

Although the aim of the pre-coating treatment was to provide a barrier to reaction between the matrix and the stainless steel during solid state consolidation, a continuous intermetallic layer was found at the coating/wire interface itself along with satellite particles in the remaining coating (Fig. 4 and Table II for EDS results). It

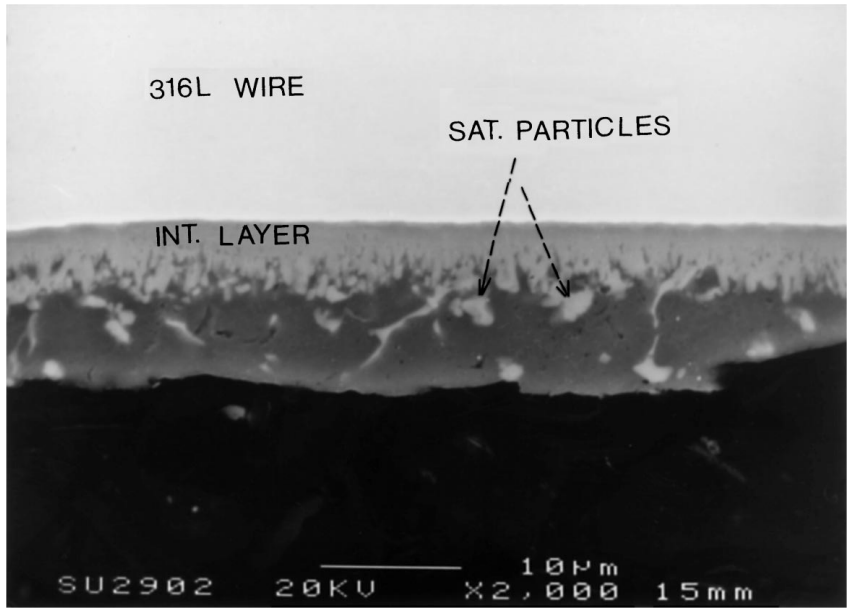

Figure 4 SEM micrograph of the A1-7.26Si coating on the 316L stainless steel wire formed during the continuous coating process at 700 °C (intermetallic layer, satellite particles).

TABLE II EDS microanalyses of the 0.5 mm coated 316L wire in Al-Si alloy at 700 °C

	316L stainless steel wires (9 analyses)		Continuous intermetallic layer (case) (7 analyses)		Satellite particles (3 analyses)		Al-Si alloy coating (6 analyses)	
Element	(wt %)[a]	(at %)	(wt %)	(at %)	(wt %)	(at %)	(wt %)	(at %)
Al	0.2 ± 0.1	0.4 ± 0.1	49.8 ± 0.5	63.7 ± 0.4	60.6 ± 6.8	72.4 ± 7.7	97.1 ± 0.9	97.5 ± 0.7
Si	0.5 ± 0.1	1.0 ± 0.1	8.4 ± 0.2	10.4 ± 0.2	7.2 ± 0.8	8.1 ± 0.3	2.2 ± 0.6	2.1 ± 0.6
Fe	69.0 ± 0.2	68.6 ± 0.2	30.6 ± 0.6	18.9 ± 0.5	27.2 ± 4.0	16.5 ± 5.7	0.7 ± 0.3	0.4 ± 0.2
Cr	17.2 ± 0.1	18.4 ± 0.1	8.7 ± 0.1	5.8 ± 0.05	3.6 ± 2.0	2.1 ± 1.0	—	—
Ni	10.4 ± 0.1	9.8 ± 0.1	1.0 ± 0.2	0.6 ± 0.1	0.9 ± 0.1	0.6 ± 0.5	—	—
Mo	2.2 ± 0.1	1.3 ± 0.04	1.2 ± 0.1	0.4 ± 0.04	0.2 ± 0.2	0.1 ± 0.1	—	—
Mn	0.5 ± 0.1	0.5 ± 0.1	0.3 ± 0.1	0.2 ± 0.03	0.3 ± 0.1	0.2 ± 0.04	—	—

95% confidence intervals.

[a]Compare with Alloy Wire Co LTDA: (C-0.029 wt %; Si-0.42 wt %; Mn-0.42 wt %; P-0.016 wt %; S-0.001 wt %; Cr-16.85 wt %; Ni-10.33 wt %; Mo-2.58 wt %).

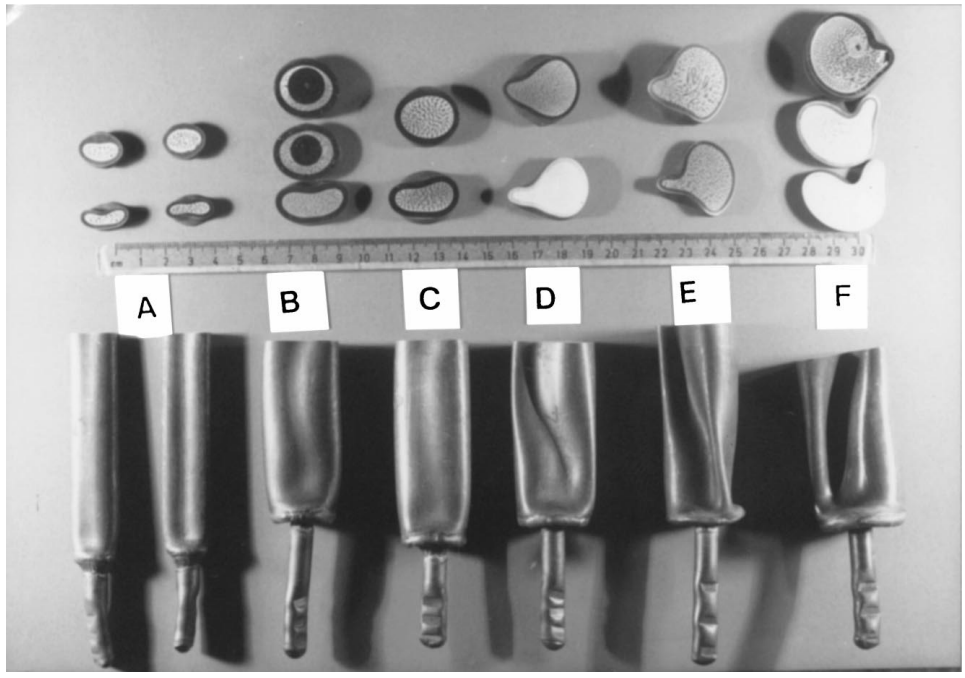

Figure 5 Longitudinal and cross-sectional views of the can after HIPping (oval/kidney shape: A, B, C), (pear shape: D, E, F, plus twisting).

is difficult to identify the interfacial reaction products unequivocally. For the continuous intermetallic layer formed during continuous coating on A17.3Si, the ratio of the at % contents in Table II suggest $A1_{11}Si_2CrFe_3$. The satellite particles have a higher A1 content and reduced amounts of Si, Fe and Cr compared to the continuous layer. The ratios correspond with $Al_{34}Si_4CrFe$. For more precise determination, TEM samples would need to be prepared and diffraction patterns analysed.

3.2. Effects of HIPping

3.2.1. Shape of can

The cans and bundles did not deform evenly during HIPing (see Fig. 5). Cans of 12 mm diameter were oval, those of 18 and 20 mm kidney-shaped and those of larger diameter (26 and 28 mm) were pear-shaped in cross-section. Longitudinally, the wider diameter cans were twisted. The dark central areas in some of the cross-sections show where the section has been taken at the can base, through part of the base itself. When the bundles were spark machined to obtain mechanical test specimens, the macroscopic effects of these deformations were clear: the fibres were no longer aligned parallel to the longitudinal axis and in addition, the twist meant that some fibres ended in the middle of a mechanical test specimen (e.g. see Fig. 3a specimen 2) The consequence is that some mechanical test specimens were unreinforced for part of their length.

3.2.2. Degree of consolidation

In general, almost full (e.g. Fig. 6 Final Stage (a)) or full (e.g. Fig. 6 Final Stage (b)) consolidation was achieved in the middle of the can. At the ends of the can, there was some constraint resisting the isotropic pressure and in some cases consolidation was incomplete. This corresponds with the intermediate stage in HIPping (e.g. Fig. 6 'Intermediate Stage' (b)). The relative density of the composite therefore tends to increase from the ends of the can towards the centre.

3.2.3. Distribution of reinforcement

Fig. 7 illustrates the effect of HIPping on a (W-M-M-W) bundle. The stainless steel reinforcement wires are not uniformly spaced through the cross-section and in several places are touching. Where three stainless steel wires touch, porosity tends to be present in the interstice, and indeed, examples were found of the aluminium matrix being extruded through the space between nearly touching wires (e.g. Fig. 8). Voids are likely sites for the initiation of failure. Fig. 9 shows there is a correlation between the number of W-W contacts (as a proportion of the total number of stainless steel wires in a given area) and the wire volume fraction for various arrangements. 0.5 mm diameter reinforcement specimens have higher wire volume fractions than those with 0.3 mm diameter wires (compare (6) with (5) and (c) with (10)) but have not prevented them. The use of Al foil has significantly reduced the number of W-W contacts (compare (5) with (10)). There are instances where two adjacent stainless steel wires appear to be 'shearing'-through the foil (e.g. see Fig. 10). The flow stress of aluminium at 500 °C is 2.6 MPa [24] and hence such 'shearing' is to be expected. If this occurs, it is bound to lead to an increase in the number of W-W contacts.

3.2.4. Interfacial reactions

Interfacial reaction products were observed with bundles (6), (7) and (8). Slight reaction was found for bundles (5) and (9), but none for bundle (10).

Electron microscopy (Fig. 11) shows cracks in the intermetallic layer of a HIPped array with pre-coated

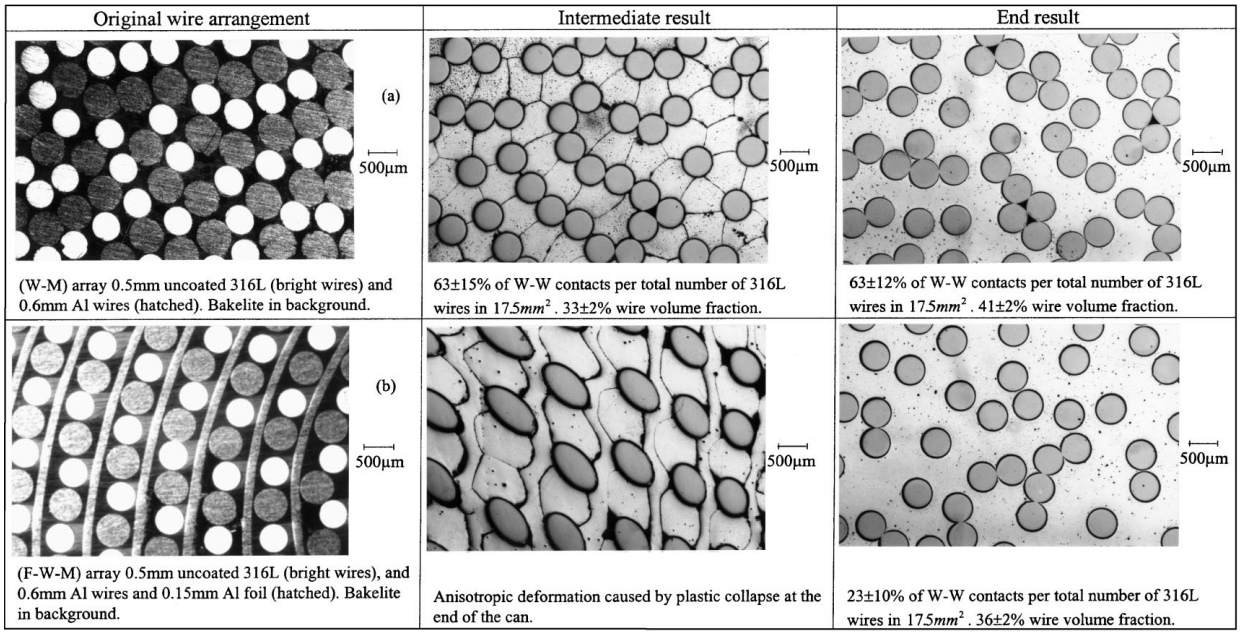

Figure 6 Cross sections showing consolidation sequences of HIPped composites for (a) (W-M) 0.5 mm 316L wires and 0.6 mm Al; and (b) (F-W-M) arrangement made of 0.15 mm Al foil, 0.5 mm 316L and 0.6 mm Al wires.

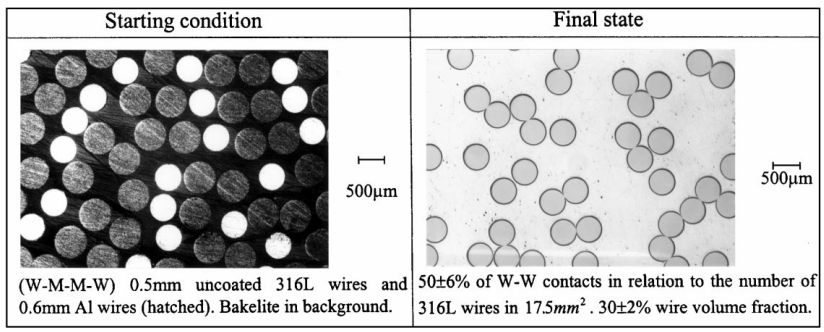

Figure 7 Cross section of the HIPped composite for the (W-M-M-W) array formed by 0.5 mm uncoated 316L wires and 0.6 mm pure Al wires. Unetched.

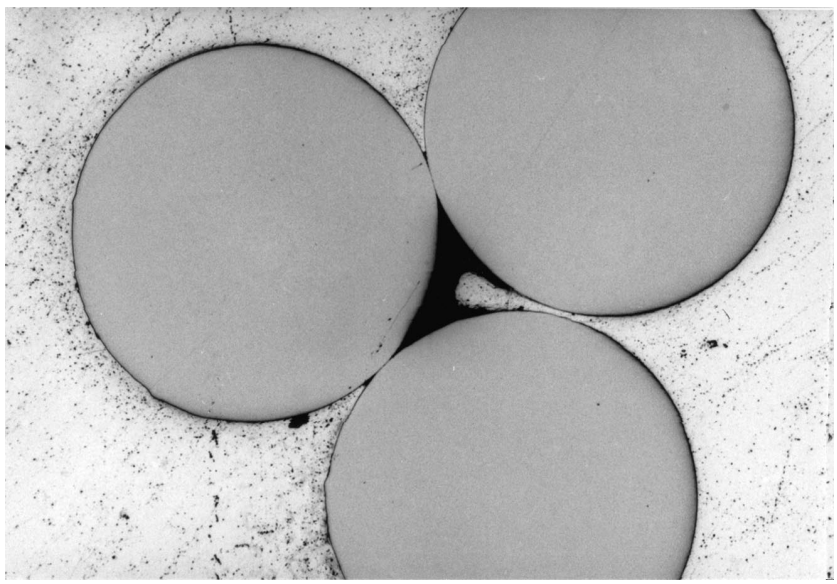

Figure 8 HIPped (W-M) 0.3 mm unocated 316L wire and 0.6 mm Al wires showing a void between the wires and matrix flowing into the void. Unetched.

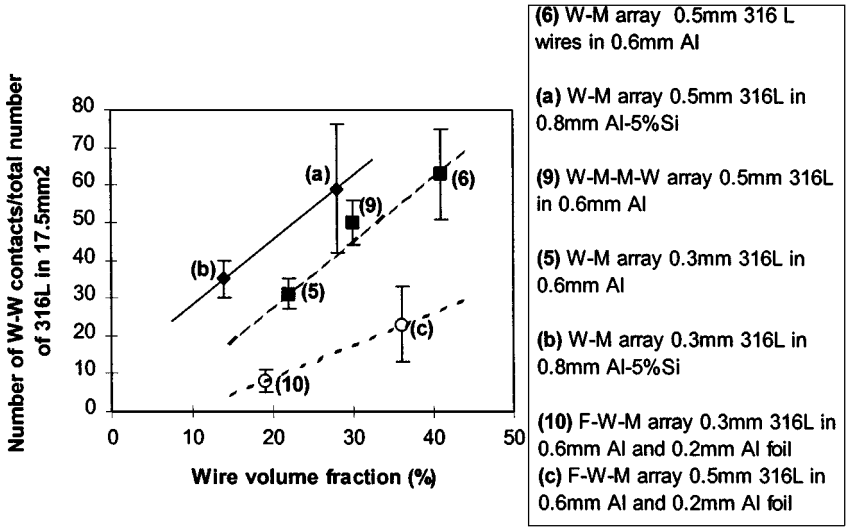

Figure 9 Effect of the wire volume fraction (%) on the number of (W-W) contacts for HIPped bundles. Bundle numbers identify with those in Table IV.

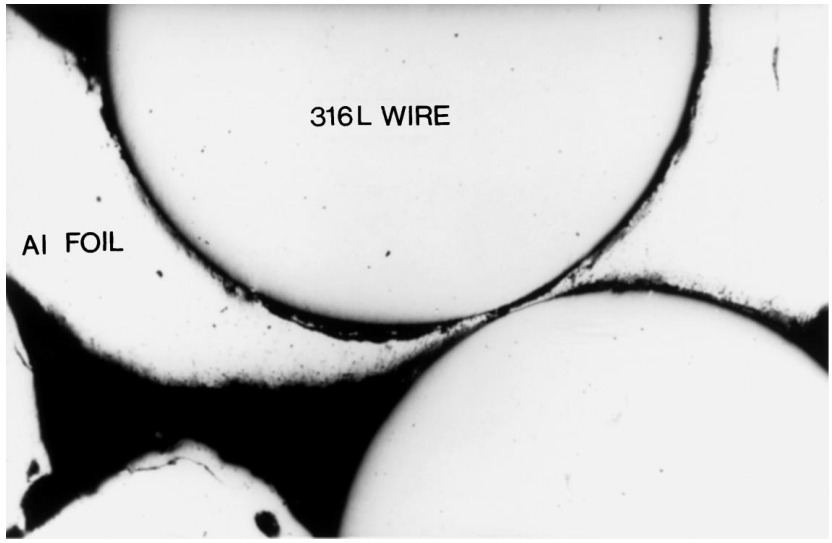

Figure 10 HIPped (F-W-M) 0.5 mm uncoated 316L wires, 0.6 mm Al wires and 0.15 mm Al foil. Al foil is being 'cut' between two 316L wires. Unetched.

wires, illustrating the brittle nature of the intermetallic. Consequently, the transfer of the HIPping pressure to the stainless steel is inefficient and this is reflected in microhardness results, with an increase for the microhardness of the uncoated wires after HIPping but not for the coated.

Bundle (6) (W-M with 0.5 mm uncoated 316L wire) had particles of reaction product (rather than a continuous layer) at specific locations along the 316L wire. Also some products of reaction had been transported into the matrix with 'flakes' of the hard drawn stainless steel (Fig. 12). However, some 316L wire flakes did not form these intermetallic products when in contact with the Al matrix. This suggests that, some flakes were easily displaced from the 316L wire surface by Al wires during HIPping. However, for those which were not easily displaced reaction occurred followed by migration.

Microanalysis (EDS) was performed on the intermetallic products formed at the aluminium/316L wire interface and at a distance of approximately 2 μm from the intermetallic products into the Al matrix (see Table III). Analyses for 0.5 mm uncoated 316L stainless steel and 0.6 mm aluminium wire are also shown in the table for comparison. Substantial proportions of Si, Fe, Cr, Ni, Mo and Mn have diffused outwards from the 0.5 mm 316L uncoated wire, and Al has diffused from the matrix to form the interfacial intermetallic product. As most elements constituting the intermetallic product originated from the 316L wire, the growth profile of these products is in the direction from the 316L wire to the matrix, so that they adopt the shape of a 'single drop' or occasionally 'multiple drops' (see Fig. 12). EDS performed adjacent to these 'drops' at a distance of 2 μm into the matrix indicated a slight increase in Fe and Cr. These elements form a solid solution with the aluminium matrix. Other elements (Si, Ni, Mo and Mn) remained in the 'drops'. The presence of Fe and Cr ahead of the 'drops' suggests that their growth is associated with diffusion of these elements.

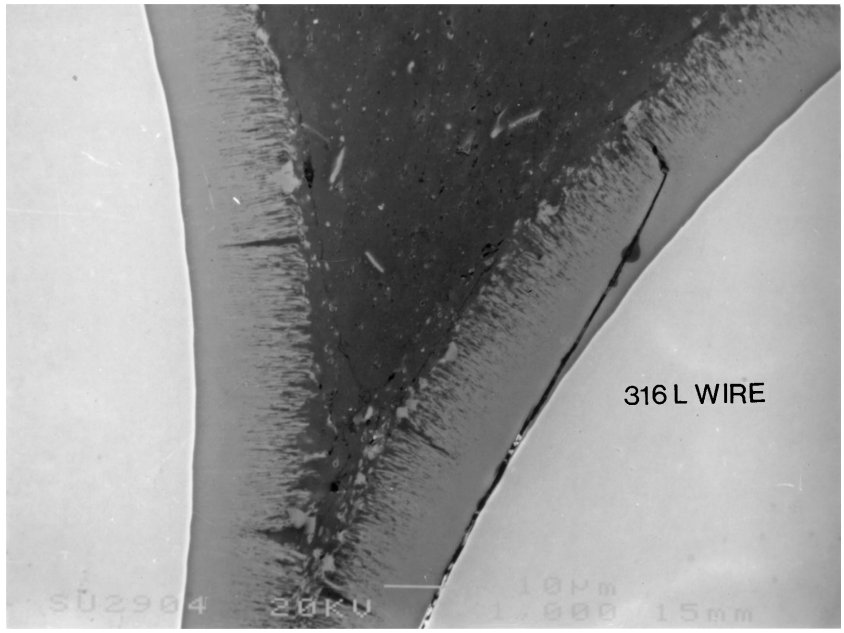

Figure 11 SEM of a HIPped composite composed of a (W-M) array 0.5 mm coated 316L wire and Al wire. Unetched.

TABLE III Results of EDS microanalyses carried out on the components and on the intermetallic products at the reinforcement/Al interface of a HIPped W-M array composed of 0.5 mm uncoated 316L wire and 0.6 mm Al wire (wire volume fraction $41 \pm 2\%$) (see Fig. 12)

	0.5 mm 316L stainless steel wire (9 analyses)		Intermetallic products at interface (7 analyses)		Al matrix at $\approx 2\ \mu$m from intermetallic products (9 analyses)		Al wire (10 analyses)	
Element	(wt %)	(at %)	(wt %)	(at %)	(wt %)	(at %)	(wt %)	(at %)
Al	0.2 ± 0.1*	0.4 ± 0.1	46.6 ± 0.7	64.2 ± 0.7	98.8 ± 0.3	99.5 ± 0.1	99.7 ± 0.2	99.8 ± 0.1
Si	0.5 ± 0.1	1.0 ± 0.1	0.4 ± 0.1	0.5 ± 0.1	—	—	—	—
Fe	69.0 ± 0.2	68.6 ± 0.2	37.0 ± 0.8	24.6 ± 0.6	1.0 ± 0.3	0.4 ± 0.08	0.3 ± 0.1	0.2 ± 0.04
Cr	17.2 ± 0.1	18.4 ± 0.1	9.0 ± 0.2	6.4 ± 0.1	0.2 ± 0.1	0.1 ± 0.01	—	—
Ni	10.4 ± 0.1	9.8 ± 0.1	5.6 ± 0.3	3.6 ± 0.2	—	—	—	—
Mo	2.2 ± 0.1	1.3 ± 0.04	1.2 ± 0.1	0.5 ± 0.03	—	—	—	—
Mn	0.5 ± 0.1	0.5 ± 0.1	0.2 ± 0.1	0.2 ± 0.1	—	—	—	—

*95% confidence interval.

Based on stoichiometry, the intermetallic products at the interface ('drops') have a formula $Al_{18}Cr_2NiFe_7$ and also contain Mo and Mn. According to Nishida and Narita [25], the microhardness of the intermetallic compounds would be in a range of approximately 760 to 850 VHN.

Contrary to the (W-M) 0.5 mm uncoated 316L bundle, the transport of 'flakes' into the matrix did not occur in the (W-M-M-W) bundle even though it has the same constituents. Furthermore, fractographs after tensile failure show flakes still adhered to the 316L wire surface.

3.3. Mechanical properties

3.3.1. Tensile testing

The stress-strain curves (Fig. 13) show that HIPped composites made from coated wire have substantially more ductility than those made from uncoated wire, for comparable volume fractions (see Table IV). Comparing bundles (7) and (8) which are both for coated wires with similar volume fractions, the bundle with the narrower diameter can (7) has a higher modulus as well as maximum uniform strength, probably because of the better wire alignment after HIPping.

Table IV shows the measured mechanical properties in comparison with predictions based on the Rule of Mixtures (ROM). There is good agreement with the predictions for: maximum uniform stress for bundles (6) and (7); elastic modulus for bundles (9) and (10); strain to failure for bundles (7) and (8). Overall though, bundle (10) gave the most consistent set of results in terms of approaching the ROM predictions. The best values for strength and modulus were obtained with bundle (6).

SEM of the fracture surfaces reemphasises the brittle nature of the intermetallic reaction product formed on coated reinforcements, with cracking occurring through that layer. All specimens shown in Fig. 13 show interfacial delamination between the constituents, between the stainless steel wires and the aluminium matrix (e.g. Fig. 14), between aluminium wires and at aluminium wire/foil interfaces. For specimens (6), (7) and (8) in Fig. 13, intermetallic reaction products are evident but these are absent for (10) (compare Figs 14 and 15 looking for the 'pimples' on the surface of the

Formation of intermetallic compounds on the 316L wire surface. These intermetallic compounds are also formed at the 316L flakes transported to the Al matrix between the Al wire boundary. Some 316L flakes are transported easily by the Al matrix and, therefore, products of reaction are not observed. ⊢—⊣ 10μm	
Intermetallic products at the interface. Flakes are observed transporting these into the Al matrix.	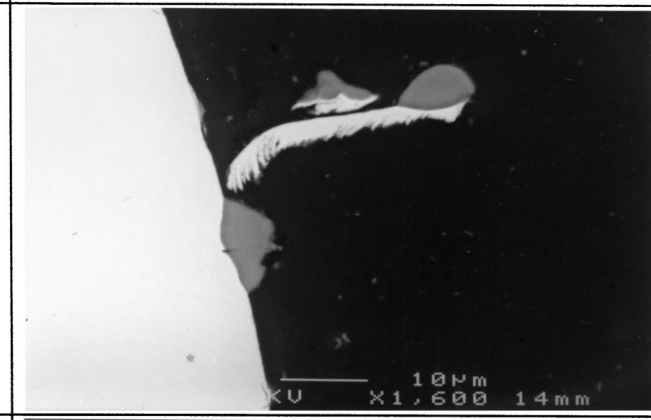
Occasionally, islands of intermetallics on the 316L wire surface tend to join and grow. Some flakes act as nucleants for the formation of intermetallic products. ⊢—⊣ 10μm	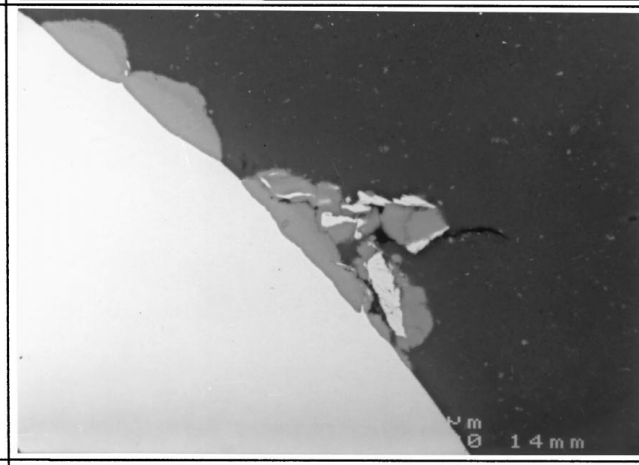
A thin flake is indicated by an arrow on the 316L wire. Intermetallic products are also observed moving with flakes into the matrix. ⊢——⊣ 10μm	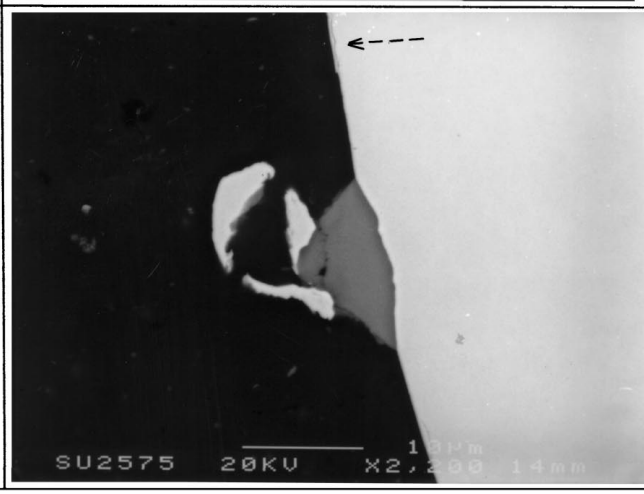

Figure 12 Backscattered electron images (SEM) of the HIPped (W-M) system composed of 0.5 mm 316L and 0.6 mm Al showing the microstructure of intermetallic products (light grey contrast), Al matrix (dark grey contrast), 316L wire and 316L flakes (bright contrast).

TABLE IV A comparison of mechanical properties of 0.5 mm (coated and uncoated) and 0.3 mm 316L/aluminium alloy composites with those of the matrix and reinforcements

Bundle constituents and HIPped bundle arrays	Volume fraction wires, $\bar{V}_f$ (%)	Maximum uniform stress, $\bar{\sigma}$(MPa)		Elastic modulus, $\bar{E}$ (GPa)		True uniform elongation $\bar{\varepsilon}$ (%)	
	Average 6 samples	Average	Rule of mixture	Average	Rule of mixture	Average	Rule of mixture
Control (F-M) bundle of HIPped Al(1)	—	59 ± 8^b	—	42 ± 8^b	—	2.8 ± 0.8^b	—
0.3 mm uncoated 316L wire (2)	—	1358 ± 210^b	—	193[a]	—	1.0 ± 0.3^b	—
0.5 mm uncoated 316L wire (3)	—	1516 ± 38^b	—	193[a]	—	1.5 ± 0.4^b	—
0.5 mm coated 316L wire (4)	—	1341 ± 3^b	—	193[a]	—	1.3 ± 0.2^b	—
(W-M) 0.3 mm uncoated 316L in Al (20 mm ø can) (5)	22 ± 1	164 ± 117^b	345	38 ± 6^b	75	1.2 ± 0.3^b	2.4
(W-M) 0.5 mm uncoated 316L in Al (20 mm ø can) (6)	41 ± 2	675 ± 26^b	656	188 ± 25^b	104	0.7 ± 0.2^b	2.3
(W-M) 0.5 mm coated 316L in Al (12 mm ø can) (7)	43 ± 4	570 ± 125^c	610	19 ± 5^c	107	4.5 ± 3.0^c	2.1
(W-M) 0.5 mm coated 316L in Al (20 mm ø can) (8)	50 ± 2	265 ± 62^d	700	17 ± 5^d	118	3.8 ± 1.8^d	2.1
(W-M-M-W) 0.5 mm uncoated 316L in Al (20 mm ø can) (9)	29 ± 3	242 ± 87^b	482	76 ± 61^b	86	1.0 ± 0.5^b	2.4
(F-W-M) 0.3 mm uncoated 316L in Al (18 mm ø can) (10)	17 ± 3	366 ± 39^b	280	68 ± 15^b	68	2.0 ± 0.1^b	2.5

80% confidence interval, except for volume fraction (%) wires (95%).
[a]ASM—Metals Reference Book, Volume 3, 1993.
[b]3 samples.
[c]2 samples.
[d]6 samples.
Rule of mixtures: $\bar{P}_c = (1 - \bar{V}_f)\bar{P}_m + \bar{V}_f\bar{P}_f$ where $\bar{P}$ is an average mechanical property ($\bar{\sigma}$, $\bar{E}$ or $\bar{\varepsilon}$), $\bar{V}$ is an average volume fraction, and the subscripts c, m, and f refer to the composite, matrix and fibre, respectively.

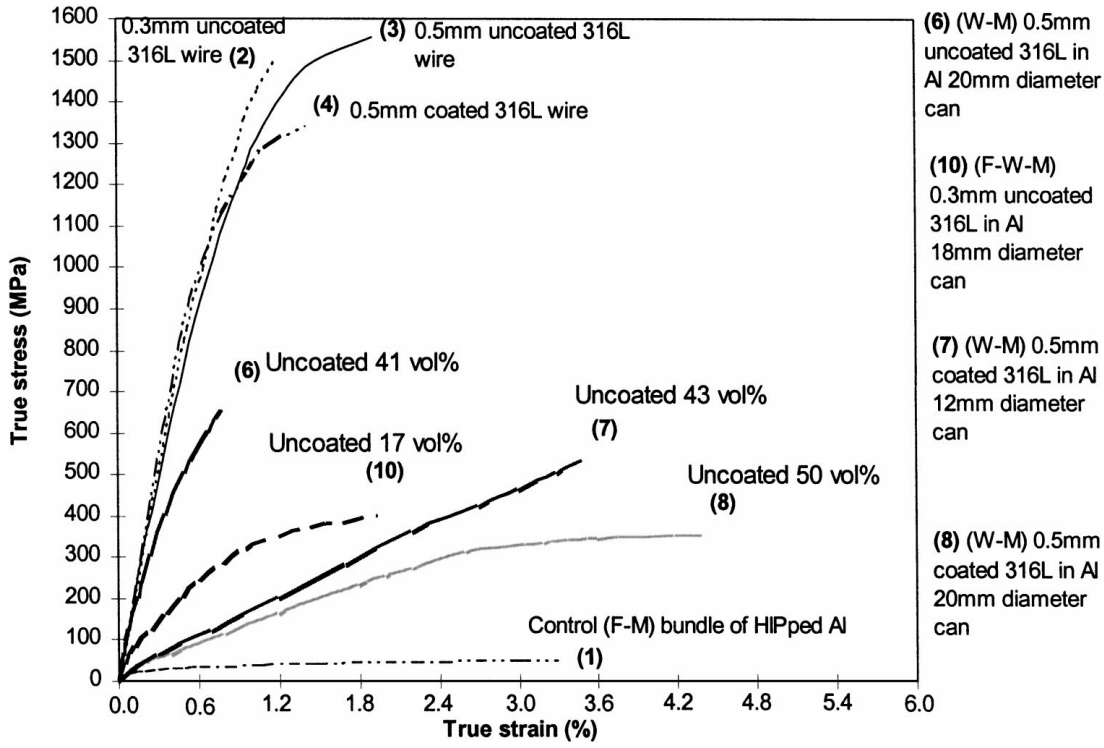

Figure 13 True stress-strain curves for (W-M) and (F-W-M) HIPped composites and for their constituents. Identifying numbers correspond with those in Table IV.

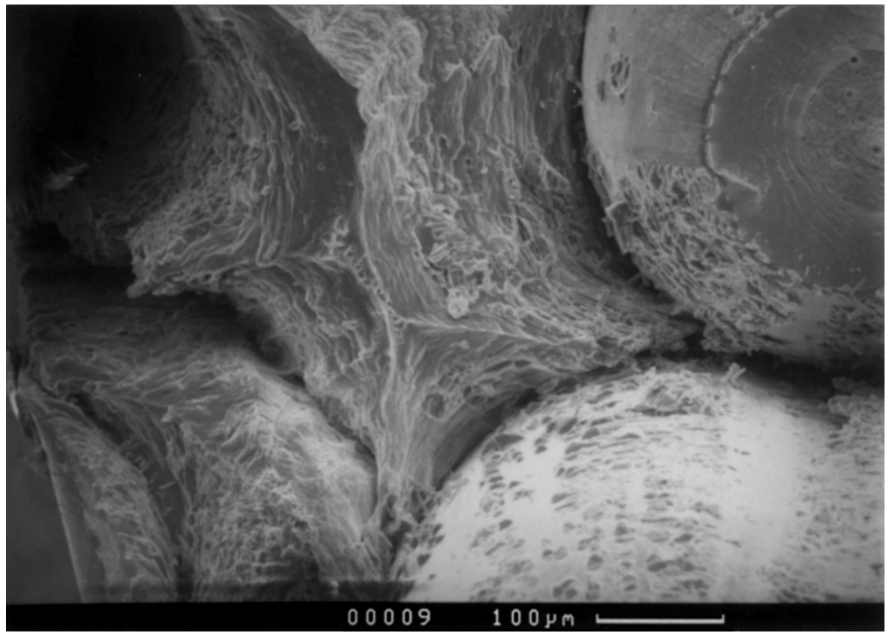

Figure 14 SEM micrograph of a tensile fracture surface of a HIPped (W-M) array 0.5 mm uncoated 316L wire and 0.6 mm Al wire composite, showing the 'cup-and-cone' fracture of the wire, the extensive matrix shearing fracture and Fe-Al particles formed along the 316L wire surface. Bundle (6) in Fig. 13.

Figure 15 SEM micrograph of a fracture surface produced by tensile testing of a HIPped (F-W-M) 0.3 mm uncoated 316L wire, 0.6 mm Al wire and 0.15 mm thick Al foil, showing a smooth surface on the 316L wire, characteristic of the absence of products of reaction. Total interfacial delamination between constituents is observed. Bundle (10) in Fig. 13.

wires). The stainless steel wires generally fail in a cup and cone manner. Some fracture surfaces also show wire misalignment.

3.3.2. Fatigue testing

The fatigue test results are shown in Fig. 16 with the best fit line between the points. The fatigue results lie in a band whose range is defined respectively by the (W-M) 0.5 mm uncoated 316L and (W-M) 0.5 mm coated 316L. Both were HIPped in a 20 mm diameter can. In spite of relatively high maximum uniform stress (see Table IV) bundle (10) ((F-W-M) array 0.3 mm uncoated 316L wires) has very poor fatigue endurance and was not included in Fig. 16. These poor fatigue endurance results may be due to the observed poor diffusion bonding between the constituents (Fig. 15). SEM analysis of the fracture surface for (W-M) 0.5 mm uncoated 316L with 0.6 mm Al wire (the material with the highest resistance to fatigue) shows virtually no fibre pullout and a strongly bonded interface between the constituents (Fig. 17). Cracks can be observed in the matrix, running perpendicular to the 316L wire with little evidence of interfacial failure. This suggests that the diffusion bonding achieved after HIPping between stainless steel and the Al matrix is sufficiently strong that the fatigue

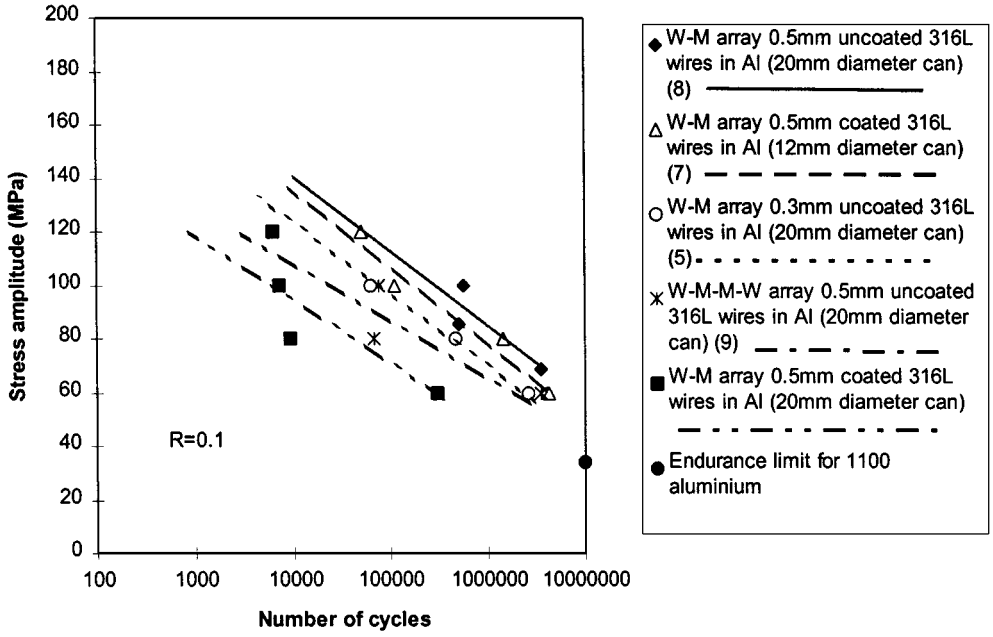

Figure 16 S-N curves of 0.3 mm and 0.5 mm uncoated and coated 316L wire/pure aluminium matrix. Bundles numbers refer to Table IV.

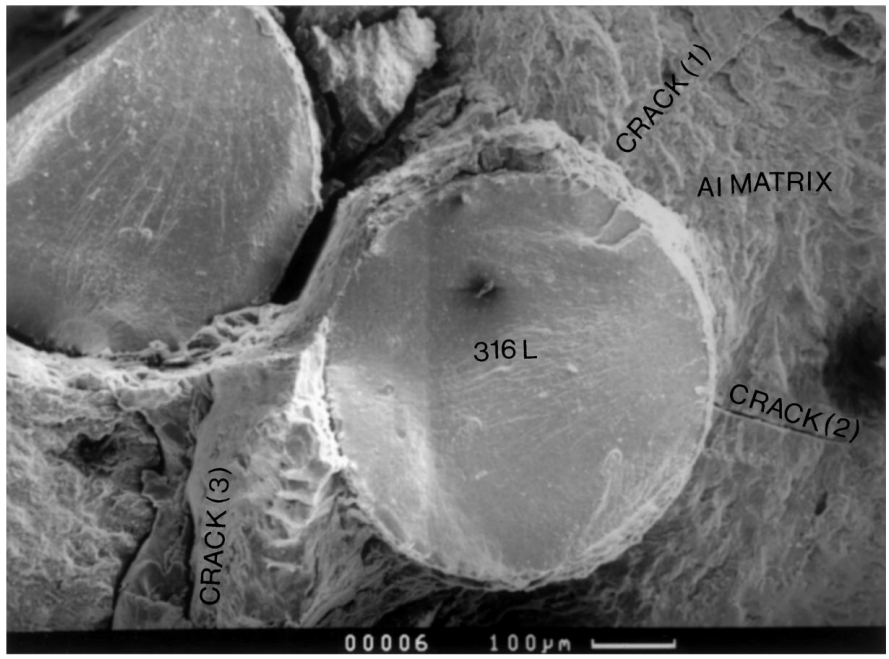

Figure 17 SEM fractograph of a fatigue specimen from a (W-M) 0.5 mm uncoated 316L wires in Al (bundle (6) in Table IV). This type of fatigue is indicative of good bonding between wire (316L) and matrix (Al). Cracks indicated as (1), (2) and (3) in the Al matrix, have apparently formed at the boundary between 0.6 mm Al wires which are only weakly diffusion-bonded after HIPping.

cracks mainly propagate perpendicular to the loading direction without deflecting to the longitudinal direction at the reinforcement-matrix interface.

Fig. 18 shows the development of the fatigue crack in the same specimen as illustrated in Fig. 17. The cracks originate at edge defects and propagate through the composite. Many microcracks are formed at the edge of the specimen (Region I), because of the lack of constraint; these are distributed in a regular pattern. The cracks propagate readily up to the first 316L wire, which then acts as a barrier to further propagation. At the same time, deformation also occurs, but with less intensity due to the greater constraint, in the other part of the matrix which is confined between the wires (Region II). The cracks from Region I need to propagate around the wires to reach Region II. This is achieved through interfacial debonding but without delamination. The wires left in the wake of the crack, bridge the crack and thus shield the crack tip from the applied stress. Eventually, fatigue cracks independently initiate and propagate through the wire to join up with the matrix cracks. This process repeats as the main fatigue crack grows but at an accelerating rate until failure.

There are insufficient data points in Fig. 16 to draw any particular conclusions about the difference in properties between the various bundles. Wire diameter and volume fraction, can diameter and wire coating are all expected to affect the fatigue behaviour. SEM of

Low magnification SEM photograph: a large number of fine cracks are formed in Region I, they pass around and grow also parallel to the wire. Further coarse cracks are formed in Region II. De-bonding is also observed.	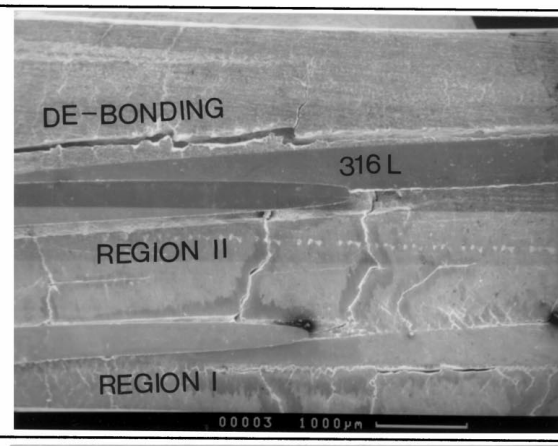
Higher magnification detail of Regions I and II. The principal cracks branch, possibly due to a wire lying beneath this plane.	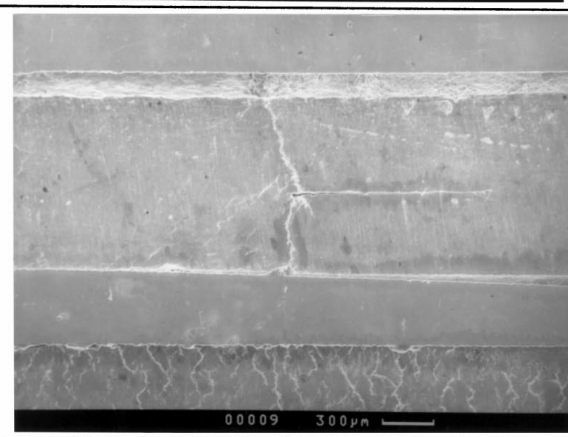
Detail of de-bonding.	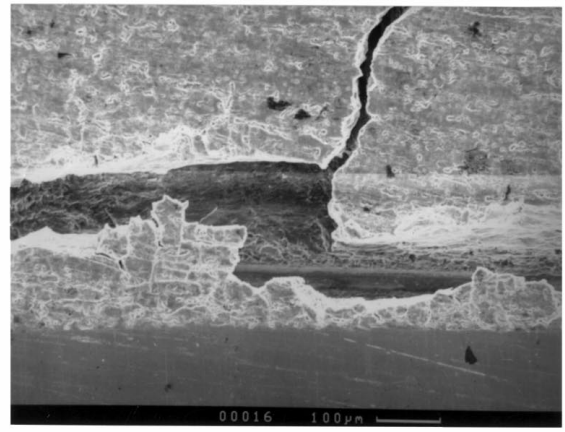
The crack path is deflected at the interface.	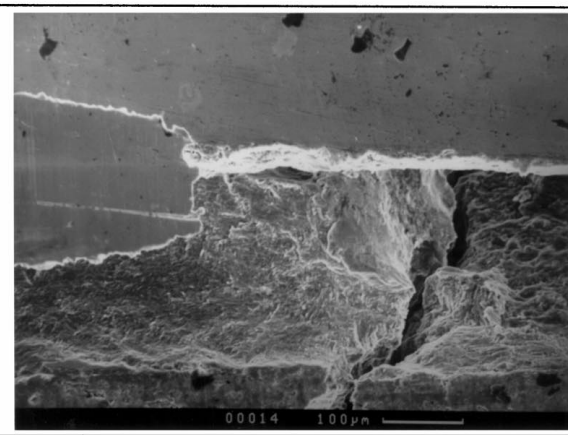

Figure 18 Series of SEM photographs taken along the gauge length of a fatigue specimen HIPped with a (W-M) array of 0.5 mm uncoated 316L wire and 0.6 mm Al wire (bundle (6) in Table IV). This specimen was subjected to a high number of cycles (10^7) to failure.

the fatigue fracture surface from a bundle with coated wires shows that, in contrast with a bundle with uncoated wires, the cracks tend to run approximately parallel to the reinforcement wires, rather than perpendicular. There is total interfacial delamination between the coating and the matrix, whereas the interface between the coating and the reinforcement tends to remain intact. For both coated and uncoated reinforcement, some

wires stretched to failure during fatigue testing. This contrasts with ceramic reinforced MMCs where the fibres fracture at weak points and then pull out of the matrix.

4. Discussion

4.1. Shape of can after HIPping

According to Juvinall [26] who analysed the stress distribution in cylinders subjected to isostatic stress, the can should fail laterally first and compress the bundle longitudinally. The can ends will then fail. In transverse cross-section, the possible plastic collapse modes can be schematised as in Fig. 19 (an extension of the treatment by Timoshenko and Gere [27]). Buckling and collapse mode 1 represent the most constrained cases.

Fig. 19 can be compared with Fig. 5. The failure by plastic collapse of tubes under pressure depends on the radial deflection resulting in an elliptical shape. At points A, B, C and D the bending moment is zero and the maximum moment occurs at $\theta = 0$ and at $\theta = \pi$.

The smaller diameter cans are more constrained than the larger diameter. Therefore, they deform by buckling and collapse modes 1 and 2. The larger diameter cans are less constrained and therefore give the pear shape i.e. collapse mode 3 and also show the longitudinal twist because of matrix plastic deformation. In general, the fibres will tend to be better aligned in the narrower diameter cans after HIPping.

The pressure required to produce plastic can collapse can be calculated as a function of the distance from the lid (see Fig. 20) by using the analysis of Haydl and Sherbourne [27] for various diameter cans. From the figures, it can be seen that the can bottom will yield before the material closest to the lid and also that this yielding pressure is not achieved for the narrowest diameter can

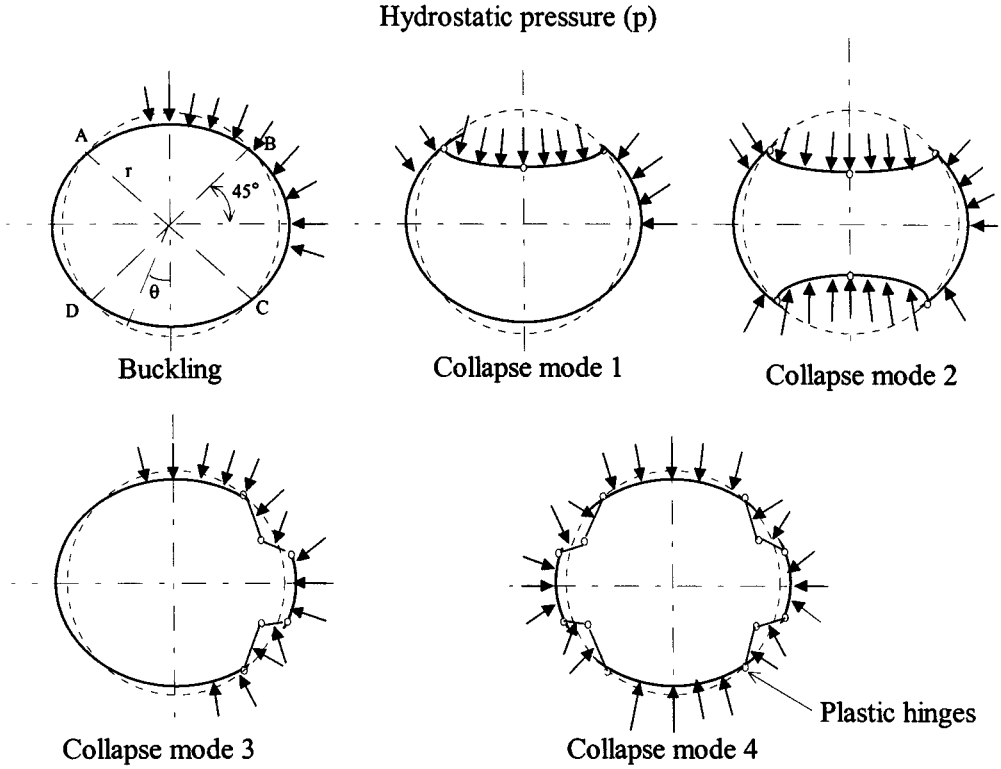

Figure 19 Possibilities for can plastic collapse in cross-section view.

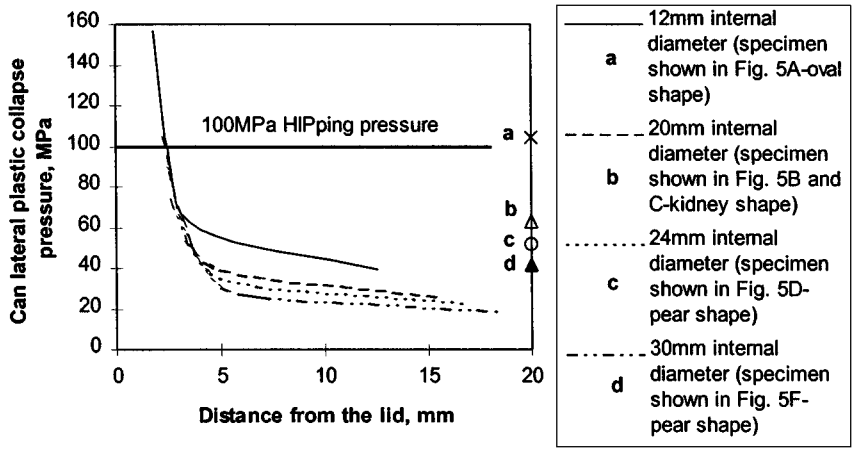

Figure 20 Calculated pressures for can lateral plastic collapse and bottom yielding pressure (a, b, c, and d).

with the HIPping cycle used in this work (HIPping pressure 100 MPa). Where lid plastic collapse does occur, it causes wire misalignment towards the ends. The variation in can lateral yielding pressure along the length will result in better consolidation in the middle than at the ends of the can.

4.2. Mechanical testing

The stress-strain curves show that HIPped composites made from coated wire show substantially more ductility than those made from uncoated wire (Fig. 13). The bundle in the narrower diameter can (7) is also stiffer and stronger than (8), probably because the reinforcement wires are better aligned. The increase in ductility with coating might be explained as follows. The brittle interface means that load transfer from the matrix to the reinforcement is less efficient than in the uncoated case. The coating then acts as a 'lubricant', fracturing at low loads and thus delaying matrix elastic deformation and consequently matrix plastic deformation. The delay continues until the whole interface has fractured on each wire under stress. After total interfacial failure, the matrix deforms plastically and then fails with limited wire reinforcement. Bundle (6) is essentially stiffer and stronger than bundle (10) because the volume fraction of reinforcement is higher (see Table IV).

Predictions of maximum uniform stress, modulus and elongation to failure using the Rule of Mixtures are in some cases comparable to experimental results but not in others. The Rule of Mixtures is rather crude for plastic phenomena but should be a good guide for an elastic property such as elastic modulus. In practice, the main reason why the measured properties are lower than those calculated in the work described here, is because the reinforcement wires are misaligned and in some cases not continuous through the bundle i.e. giving a lower effective volume fraction than should be the case. In addition, where diffusion bonding is inadequate, the modulus and strength will be low because the material behaves more like an aggregate than a continuous solid.

The Scanning Electron Microscopy results from tensile fracture surfaces show that failure was in some cases through the original boundaries between the constituents suggesting that complete diffusion bonding has not been achieved, particularly where residual alumina is present between the aluminium constituents. Better bonding might be achieved by lengthening the time at temperature and pressure in the HIPping cycle. This would also lead to a greater degree of interfacial reaction which, in view of the test results, is beneficial, i.e. bundle (6) with a significant degree of interfacial reaction gives better mechanical properties than bundle (5) where the reaction is only slight. An alternative approach might be to outgas the cans and their contents more thoroughly before welding by heating the can gently whilst under vacuum. The fatigue results provide evidence that the bond between the coating and the reinforcement for coated wires is a strong one.

The fatigue failure mechanism has been discussed in Section 3.3.2. There are insufficient data points in Fig. 16 to draw firm conclusions. Bundles with coated wires would be expected to give poorer fatigue behaviour than those with uncoated wires, because the brittle interface around the reinforcement would provide little resistance to the crack tip propagating around the reinforcing wire. Smaller diameter reinforcing wires would tend to give poorer performance because they would give less effective crack bridging than wider diameter wires. Poorer performance would also be associated with lower volume fractions as there would be less crack tip plasticity constraint and fewer fibres bridging the crack. Wire misalignment, wire discontinuity and voids between wires will all reduce the fatigue endurance.

5. Summary and conclusions

Metal reinforced Metal Matrix Composites (MMMCs) have been made by Hot Isostatic Pressing (HIPping) 316L stainless steel wires with an aluminium matrix at 525 °C/120 min/100 MPa. Some stainless steel wires were pre-coated with Al7Si to examine its effect on properties. During the HIPping the mild steel cans collapse unevenly to give different cross-section shapes, and for larger diameter cans there was also some longitudinal twisting. Wires tend to be better aligned after HIPping in the narrower diameter cans, giving higher modulus and UTS. High reinforcement volume fractions tend to give better fatigue properties. Coated reinforcement gives higher composite elongation to failure than uncoated, possibly because of the loss of load transfer brought about by the extensive cracking of the brittle coating. This may occur in the final stage of failure which is negligible in fatigue terms. Stainless steel reinforcements fail by fatigue. Cracks form and propagate independently in the wires and eventually they join with the matrix fatigue cracks. This contrasts with ceramic reinforced MMCs where fibres fracture at weak points and then pull out of the matrix. Interposing foils between layers of wires reduces the number of wire-wire contacts but does not prevent them. Better results might be obtained by improving the distribution of the constituents of the can prior to HIPping, longer HIPping times (to improve the diffusion bonding) and optimisation of the geometry of the can so as to give good reinforcement alignment. If ductility is required, coated fibres are an advantage.

Acknowledgements

We are grateful to Bodycote HIP for the provision of facilities and to CNPq and UNESP of Brazil for support for A. Lima Filho.

References

1. F. BARBIER and M. H. AMBROISE, in Proceedings ICCM/VIII Composites: Design and Application, Honolulu, July 15–19 1991, edited by S. W. Tsai and G. S. Springer (Stanford University), Section 12–21, pp. 18J1.
2. P. J. E. FORSYTH, R. W. GEORGE and D. A. RYDER, *Appl. Mater. Res.* (Oct. 1964) 223.

3. A. A. BAKER, *ibid.* (July 1966) 143.
4. LEROY W. DAVIS, *Metal Progress* **91** (1967) 105.
5. J. R. HANCOCK and J. C. GROSSKREUTZ, ASTM Special Technical Publication No. 438, (1968) 134.
6. H. R. LEE, D. A. RYDER and T. J. DAVIES, *Int. J. Mech. Sci.* **12** (1970) 739.
7. W. W. GERBERICH, *J. Mech. Phys. Solids* **19** (1971) 71.
8. M. R. PINNEL and A. LAWLEY, *Met. Trans.* **1** (1970) 1337.
9. M. R. PINNEL and A. LAWLEY, *ibid.* **2** (1971) 1415.
10. A. PATTNAIK and A. LAWLEY, *ibid.* **5** (1974) 111.
11. R. B. BHAGAT, *ibid.* **16A** (1985) 623.
12. R. B. BHAGAT, *J. Mater. Sci.* **24** (1989) 1496.
13. C. COLIN, Y. MARCHAL, F. BOLAND and F. DELANNAY, *J. de Physique IV* Colloque C7, supplément au Journal de Physique III, **3** (Nov. 1993) 1749.
14. F. DELANNAY, C. COLIN, Y. MARCHAL, L. TAO, F. BOLAND, P. COBZARU, B. LIPS and M. A. DELLIS, *ibid.* 1675.
15. K. BAN and T. ARAI, Method of producing a unidirectional fiber-reinforced composite material, U.S. Patent 4,266,596, May 12, 1981, Honda Giken Kogyo Kabushiki Kaisha, Tokyo, Japan.
16. R. L. TRUMPER, *Metals and Materials* (Nov. 1987) 662.
17. Y.-H. HWANG, C.-F. HORNG, S.-J. LIN, K.-S. LIU and M.-T. JAHN, *J. Mater. Sci.* **32** (1997) 719.
18. Y.-H. HWANG, C.-F. HORNG, S.-J. LIN, K.-S. LIU and M.-T. JAHN, *Mater. Sci. Technol.* **13** (1997) 982.
19. SHOU-YI CHANG and SU-JIEN LIN, *J. Mater. Sci.* **32** (1997) 5127.
20. R. IRMANN, *Aluminum* **33**(4) (1957) 250.
21. H. V. ATKINSON and B. A. RICKINSON, Hot Isostatic Processing, Published Adam Hilger in series on New Manufacturing Processes and Materials, 1991, 190 pp.
22. A. BERGHEZAN, *Composites* (Sept. 1972) 200.
23. I. GREAVES, M. V. HARTLEY, R. J. LEE, M. S. FOUND and J. R. YATES, in Proc 2nd International Seminar (Experimental Techniques and Design in Composite Materials), 7–8 September 1991, edited by M. S. Found (SIRIUS, University of Sheffield) p. 274.
24. H. R. VOORHEES and J. W. FREEMAN, ASTM Special Technical Publication No. 291, 1960.
25. K. NISHIDA and T. NARITA, *Trans. Japan Inst. Metals* **14** (1973) 431.
26. R. C. JUVINALL, "Engineering Considerations of Stress, Strain, and Strength" (McGraw-Hill Book Company, New York, 1967).
27. S. P. TIMOSHENKO and J. M. GERE, "Theory of Elastic Stability" (McGraw-Hill Book Company, New York, 1961).
28. H. M. HAYDL and A. N. SHERBOURNE, *J. Engineering for Industry* (Feb. 1973) 215.

Received 14 September
and accepted 15 September 1998